Endosomolytic Nano-Polyplex Platform Technology for Cytosolic Peptide Delivery To Inhibit Pathological Vasoconstriction

Brian C. Evans,[†] Kyle M. Hocking,[†] Kameron V. Kilchrist,[†] Eric S. Wise,[‡] Colleen M. Brophy,[‡,§] and Craig L. Duvall*[,†]

[†]Department of Biomedical Engineering, Vanderbilt University, 2301 Vanderbilt Place, PMB 351826, Nashville, Tennessee 37235, United States, [‡]Division of Vascular Surgery, Department of Surgery, Vanderbilt University Medical Center, D-5237 Medical Center North, 1161 22nd Avenue South, Nashville, Tennessee 37232, United States, and [§]Veterans Affairs Medical Center, VA Tennessee Valley Healthcare System, 1310 24th Avenue South, Nashville, Tennessee 37212, United States

ABSTRACT A platform technology has been developed and tested for delivery of intracellular-acting peptides through electrostatically complexed nanoparticles, or nano-polyplexes, formulated from an anionic endosomolytic polymer and cationic therapeutic peptides. This delivery platform has been initially tested and optimized for delivery of two unique vasoactive peptides, a phosphomimetic of heat shock protein 20 and an inhibitor of MAPKAP kinase II, to prevent pathological vasoconstriction (*i.e.*, vasospasm) in human vascular tissue. These peptides inhibit vasoconstriction and promote vasorelaxation by modulating actin dynamics in vascular smooth muscle cells. Formulating these peptides into nano-polyplexes significantly enhances peptide uptake and retention, facilitates cytosolic delivery through a pH-dependent endosomal escape mechanism, and enhances peptide bioactivity *in vitro* as measured by inhibition of F-actin stress fiber formation. In comparison to treatment with the free peptides, which were endowed with cell-penetrating sequences, the nano-polyplexes significantly increased vasorelaxation, inhibited vasoconstriction, and decreased F-actin formation in the human saphenous vein *ex vivo*. These results suggest that these formulations have significant potential for treatment of conditions such as cerebral vasospasm following subarachnoid hemorrhage. Furthermore, because many therapeutic peptides include cationic cell-penetrating segments, this simple and modular platform technology may have broad applicability as a cost-effective approach for enhancing the efficacy of cytosolically active peptides.

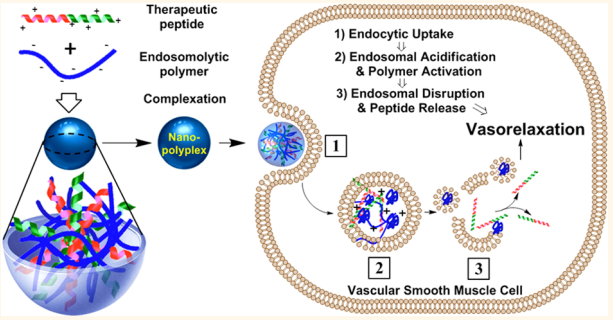

KEYWORDS: nanoparticle · polyplex · peptide · drug delivery · endosomal escape · vasospasm

The therapeutic potential of peptides to treat pathologies such as cancer and vascular disease has continually increased as a result of the elucidation of the fundamental, molecular-level disease etiology.[1−4] Peptides are especially attractive due to their increased specificity, biocompatibility, and solubility in contrast to the small molecule drugs that dominate the current pharmaceutical market. Despite these advantages, there is a lack of effective delivery technologies that can circumvent the numerous anatomical and metabolic barriers present *in vivo* that limit intracellular delivery of peptides; peptides generally have short half-lives, suffer from proteolytic degradation, lack the ability to translocate the cell membrane, and have poor intracellular bioavailability due to entrapment within the degradative/recycling vesicles of the endolysosomal trafficking pathways.[5−8] Approaches previously explored to overcome these barriers have included altering peptide chemistry to improve proteolytic resistance and *in vivo* half-life[9−11] and use of electroporation or cell-penetrant/fusogenic peptides to increase cellular internalization.[12−14] The development of colloidal drug carriers such as liposomes, micelles, and nanoparticles for delivery of biomacromolecular therapeutics has also increased dramatically in the past decade.[15−17] Despite these advances, there are no examples of nanocarrier formulations for intracellular

* Address correspondence to craig.duvall@vanderbilt.edu.

Received for review January 22, 2015 and accepted May 24, 2015.

Published online May 25, 2015
10.1021/acsnano.5b00491

peptide delivery that have been simple, robust, and scalable enough to justify translation for clinical use. Thus, the goal of this work is to develop a simple, generalizable peptide drug delivery nanoformulation to enhance the cellular uptake, endosomal escape, intracellular retention, and bioactivity of therapeutic peptides.

While therapeutic peptide delivery has the potential to impact numerous biomedical applications, in this work, initial development and testing has been focused on delivery of vasoactive peptides to prevent pathological vasoconstriction (*i.e.*, vasospasm) in human vascular tissue. The clinical burden of vasospasm can be highlighted in two areas: (1) coronary vasospasm following coronary artery bypass grafting and (2) subarachnoid hemorrhage-induced symptomatic cerebral vasospasm. There are approximately 1.6 million coronary artery bypass procedures performed annually in the United States,[18] and acute coronary vasospasm occurs in 1−8% of all patients undergoing coronary artery bypass grafting.[19] Treatment of coronary vasospasm includes immediate, invasive intracoronary administration of vasodilators such as nitroglycerin or verapamil.[20] The approach described here would be less invasive and would be applied prophylactically (intraoperatively) prior to grafting. Similarly, the current treatments for symptomatic cerebral vasospasm following subarachnoid hemorrhaging are also limited. Subarachnoid hemorrhages (SAH) affect 30000 people annually and cause up to 7% of all strokes.[21] Nearly all cases of SAH are due to rupture of a cerebral aneurysm, and 40−50% of post-SAH mortality is attributed to symptomatic vasospasm (*i.e.*, delayed cerebral ischemia).[22] Current therapeutic approaches (*i.e.*, triple H therapy)[23] have yielded no significant improvement in mortality rates. Since cerebral perfusion pressure is directly proportional to mean arterial pressure, systemically delivered vasodilators are avoided as they result in systemic hypotension, thereby exacerbating cerebral ischemia. Thus, a therapeutic intervention that avoids systemic effects by selectively targeting vasospastic vessels may represent a promising approach to treat pathological vasoconstriction.

The current studies are focused on delivery of two vasoactive peptides that affect actin dynamics in vascular smooth muscle as a means to modulate vessel contraction and relaxation. Smooth muscle contraction is caused by the sliding of actin and myosin filaments past each other within smooth muscle cells. Based on this mechanism, actively depolymerizing or destabilizing actin filaments results in inhibition of smooth muscle contraction and enhancement of relaxation as the myosin filaments no longer have an intact substrate to bind to and utilize to generate force. Thus, the destabilization of actin filaments in smooth muscle is a promising therapeutic approach to preventing and treating vasospasm. Vasospasm is associated with a down-regulation of heat shock protein 20 (HSP20, also known as HSPB6) and concomitant increases in the expression and phosphorylation of heat shock protein 27 (HSP27, also known as HSPB1). Both HSP20 and HSP27 are key regulators of actin dynamics and contraction in smooth muscle.[24,25] HSP20 is activated through nucleotide-dependent protein kinases and is thought to interact with the 14-3-3 scaffolding protein leading to the dissociation, dephosphorylation, and activation of the actin disassembly protein cofilin[25] (Figure 1).

Activation of MAPKAP kinase II (MK2) by p38 MAPK is also believed to contribute to vasoconstriction through the formation of filamentous actin (F-actin) stress fibers within smooth muscle cells. MK2 phosphorylates HSP27, which associates with filamentous actin to prevent actin depolymerization and inhibit tissue vasorelaxation.[26,27] Activated MK2 also phosphorylates LIM kinase which phosphorylates and deactivates cofilin, thereby inhibiting actin depolymerization.[28]

Thus, both HSP20 and MK2 play key roles in actin dynamics and represent promising targets to treat and prevent vasospasm without systemic effects on vascular tone as demonstrated in previous studies utilizing an *in vivo* model of subarachnoid hemorrhage.[29] Here, a peptide mimetic of phosphorylated HSP20 (p-HSP20) is utilized; this peptide was recently developed and shown to prevent SAH-induced macrovascular vasospasm in a noncraniotomy model of SAH-induced vasospasm.[30] In addition, a MK2 inhibitory peptide (MK2i) is pursued that was derived from a sequence shown by Hayess and Benndorf to inhibit MK2 *in vitro*.[31] This peptide sequence was optimized[32] and shown to enhance sodium nitroprusside-induced vasorelaxation of vascular smooth muscle.[33] However, sequestration and accumulation of both the p-HSP20 and MK2i peptides in the endolysosomal trafficking pathway remain significant barriers to achieving optimal bioactivity on the actin regulatory machinery located in the cytoplasm.[8] This endosomal barrier has required previous studies to utilize extremely high doses to achieve therapeutic bioactivity; improving the delivery of these peptides will achieve superior and cost-effective therapeutic efficacy.

To address this delivery limitation, we have developed a simple, translational nano-polyplex (NP) platform for the cytosolic delivery of p-HSP20 and MK2i therapeutic peptides. These NPs significantly enhance peptide uptake, enable endolysosomal escape, and enhance peptide bioactivity approximately 10-fold *in vitro* and *ex vivo*. This NP technology demonstrates potential for clinical translation to prevent vasospasm and represents a more broadly applicable pharmaceutical platform for therapeutic peptide delivery.

RESULTS AND DISCUSSION

Synthesis, Characterization, and Optimization of MK2i-NPs and p-HSP20-NPs. The MK2i peptide with the sequence

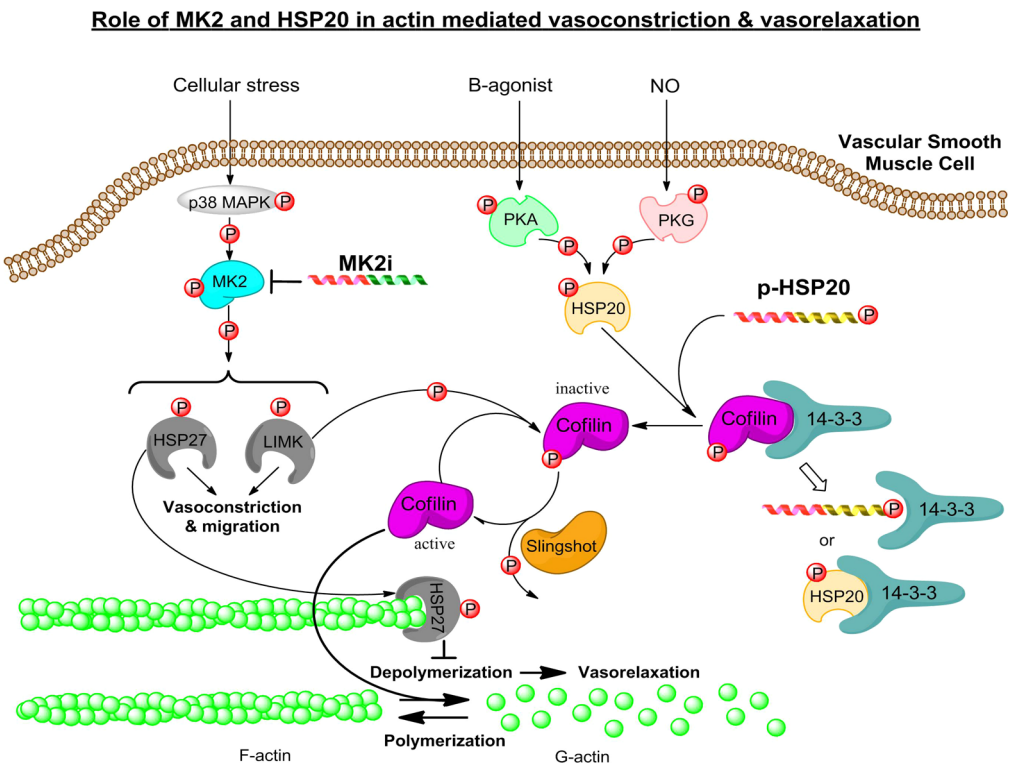

Figure 1. Mechanisms of action of MAPKAP kinase 2 (MK2) and heat shock protein 20 (HSP20) in actin-mediated vasoconstriction and vasorelaxation. MK2 is activated by cellular stress (*e.g.*, mechanical trauma, cytokines, oxidative stress, *etc.*) through p38 MAPK. Phosphorylated MK2 activates a number of downstream effectors: (1) phosphorylation of heat shock protein 27 (HSP27) results in capping of filamentous actin, thereby inhibiting actin depolymerization and vasorelaxation; (2) phosphorylation of LIM kinase (LIMK) results in phosphorylation and deactivation of cofilin, which prevents actin degradation and inhibits vasorelaxation. The MK2 inhibitory peptide (MK2i) binds to MK2, preventing the activation of these downstream effectors and promoting vasorelaxation. HSP20 is phosphorylated by cyclic nucleotide-dependent protein kinases (PKA and PKG), resulting in binding to and displacement of phosphorylated cofilin from the 14-3-3 protein. This displacement allows for cofilin to be dephosphorylated by phosphatases such as slingshot, resulting in the activation of cofilin and concomitant cofilin-mediated depolymerization of filamentous actin. The phospho-HSP20 peptide mimetic (p-HSP20) recapitulates the activity of phosphorylated HSP20, ultimately leading to vasorelaxation.

YARAAARQARA-KALARQLGVAA and the p-HSP20 peptide with the sequence YARAAARQARA-WLRRA-sAPLPGLK were synthesized *via* solid-phase synthesis, and purity was verified through electrospray ionization mass spectrometry (ESI-MS) (Supporting Information Figure S1). Reversible addition−fragmentation chain transfer (RAFT) polymerization was utilized to synthesize poly(propylacrylic acid) (PPAA) [DP = 193 (GPC), DP = 190 (^{1}H NMR), PDI = 1.47 (GPC)]. NPs were formed by simple mixing of the PPAA homopolymer with the MK2i or p-HSP20 peptides in phosphate-buffered saline (PBS) at pH 8.0, which is between the pK_a values of the primary amines present on the peptides (pK_a ∼ 9−12 depending on the amino acid residue) and the carboxylic acid moieties in the PPAA polymer (pK_a ∼ 6.7); this ensures optimal solubility and net charge on both molecules to facilitate electrostatic complexation.

To assess the impact of nanoparticle formulation conditions, a series of MK2i-NPs and p-HSP20-NPs were prepared at a range of charge ratios [*i.e.*, CR = ($[NH_3^+]_{MK2i/p\text{-}HSP20}/[COO^-]_{PPAA}$)], and the size distribution and particle surface charge were characterized through dynamic light scattering (DLS) and ζ-potential analysis, respectively. As expected, MK2i-NP and p-HSP20-NP ζ-potential was directly proportional to the CR (Figures 2A and 3A). The CR also significantly affected NP size, with a narrow range of CRs yielding a unimodal size distribution (*i.e.*, CR = 1:2 and 1:3 for MK2i-NPs, Supporting Information Table S1, and CR = 3:1 for p-HSP20-NPs, Supporting Information Table S2). A CR of 1:3 was utilized in subsequent studies for the MK2i-NP formulation, and a CR of 3:1 was utilized for the p-HSP20-NP formulation; these charge ratios consistently yielded a unimodal size distribution with minimal particle size and polydispersity (MK2i-NP D_h = 119 ± 28 nm, ζ = −11.9 ± 3.2 mV, Figure 2B; p-HSP20-NP D_h = 141 ± 6 nm, ζ = −7.5 ± 2.8 mV, Figure 3B). This difference in the charge ratio that produced unimodal particles between the two peptides may be attributable to differences in peptide size, charge distribution, sequence hydrophobicity, or secondary structures, and future analysis of a broader library of peptides will be required to better understand the structure−function relationships of these formulations. Interestingly, both optimal NP formulations demonstrated a negative ζ-potential, indicating

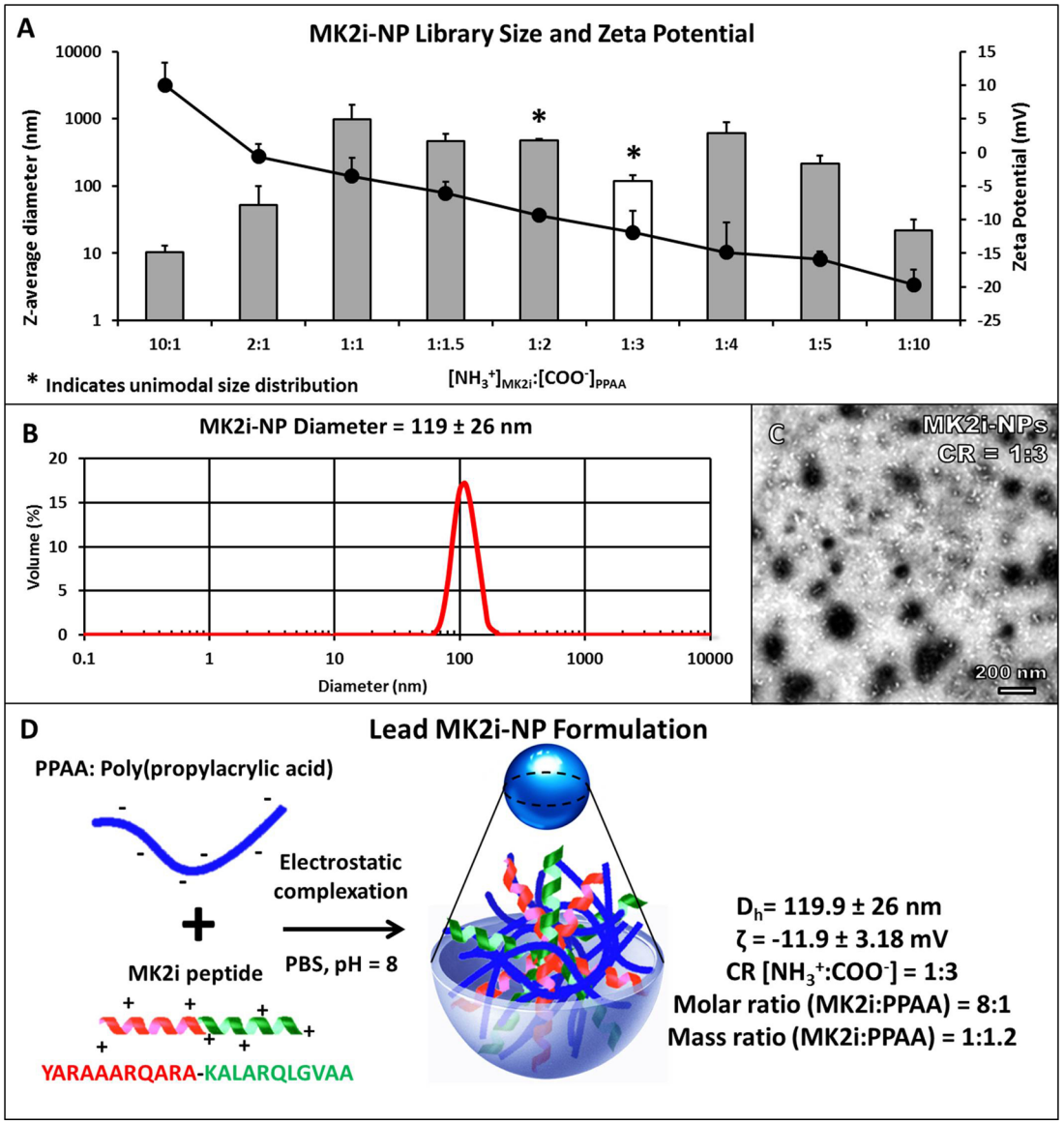

Figure 2. MK2i-NP formulation. (A) *Z*-average diameter (bars) and ζ-potential (circles) of MK2i-NPs prepared at a different charge ratios (CR = $[NH_3^+]_{MK2i}/[COO^-]_{PPAA}$). Asterisks (*) denote a unimodal size distribution, and the white bar represents the MK2i-NP formulation that yielded a unimodal size distribution with minimal size and polydispersity. (B) Representative DLS trace of lead MK2i-NP formulation (CR = 1:3). (C) Representative TEM image of uranyl acetate stained MK2i-NPs; scale bar = 200 nm. (D) Synthesis and characterization summary for lead MK2i-NP formulation. CR = charge ratio, D_h = hydrodynamic diameter, ζ = zeta-potential.

that the cationic peptides are sequestered in the core of the nano-polyplexes and the anionic PPAA polymer is more preferentially localized to the particle surface. The leading MK2i-NP and p-HSP20-NP formulations were also characterized through transmission electron microscopy (TEM) imaging (Figures 2C and 3C), which confirmed the presence of nanostructures with size distributions in accordance with DLS results. For subsequent *in vitro* and *ex vivo* studies, these lead NP formulations (Figures 2D and 3D) were compared to the corresponding free peptide.

NP *In Vitro* Biocompatibility, Uptake, Retention, Trafficking, and Bioactivity. The biocompatibility of the lead candidate MK2i-NP and HSP20-NP formulations was compared to the corresponding free peptide at a range of doses (10−500 μM peptide) in human coronary artery vascular smooth muscle cells (HCAVSMCs) *in vitro*. HCAVSMCs were treated for 2 h and then incubated in fresh medium for 24 h prior to running cytotoxicity assays. No significant cytotoxicity was evident for MK2i-NPs at all concentrations tested, whereas the free MK2i peptide demonstrated mild toxicity at the highest dose tested (76% cell viability at 500 μM, Supporting Information Figure S2). HSP20-NPs and the HSP20 peptide were found to be biocompatible with the exception of mild cytotoxicity detected at 500 μM (60 and 77% viability for p-HSP20-NPs and the free p-HSP20 peptide, respectively).

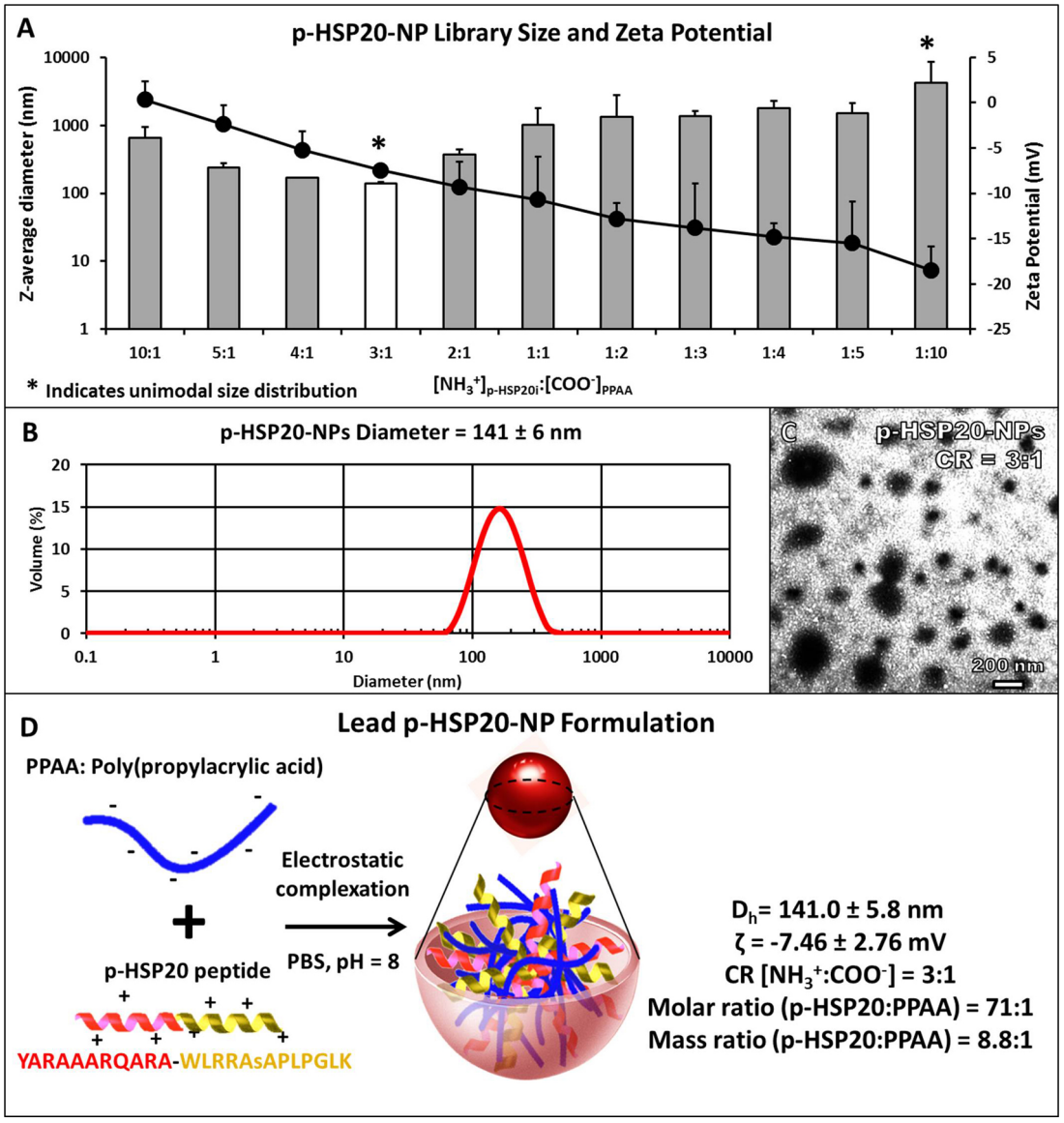

Figure 3. p-HSP20-NP formulation. (A) *Z*-average diameter (bars) and ζ-potential (circles) of p-HSP20-NPs prepared at a different charge ratios (CR = $[NH_3^+]_{p\text{-}HSP20}/[COO^-]_{PPAA}$). Asterisks (*) denote a unimodal size distribution, and the white bar represents the p-HSP20-NP formulation that yielded a unimodal size distribution with minimal size and polydispersity. (B) Representative DLS trace of lead p-HSP20-NP formulation (CR = 3:1). (C) Representative TEM image of uranyl acetate stained p-HSP20-NPs; scale bar = 200 nm. (D) Synthesis and characterization summary for lead p-HSP20-NP formulation. CR = charge ratio, D_h = hydrodynamic diameter, ζ = zeta-potential.

Quantity of MK2i-NP and p-HSP20-NP uptake and intracellular retention over time were assessed through flow cytometric analysis of HCAVSMCs treated for 30 min, washed, and maintained in fresh medium for 0 or 3 days. More than an order of magnitude increase in uptake (~70-fold increase in MK2i uptake and ~35-fold increase in p-HSP20 uptake) was detected for both peptides when incorporated into NPs (Figure 4). Since the negative ζ-potential of both NP formulations indicates that the PPAA polymer is primarily exposed at the NP surface, this increase in uptake is likely facilitated by the pH-responsive polymer. More specifically, the α-alkyl substitution of the propyl moiety imparts PPAA with lipophilic/hydrophobic character, suggesting that the observed differences in uptake may be the result of increased hydrophobic interactions of NPs with the cell membrane. In addition to increased uptake, HCAVSMCs treated with MK2i-NPs or p-HSP20-NPs demonstrated increased intracellular peptide retention 3 days after treatment removal compared to that of the free MK2i or p-HSP20 peptide (82% *vs* 54% of initial uptake remaining for MK2i-NPs *vs* free MK2i, Figure 4A; 70% *vs* 35% retention of p-HSP20-NPs *vs* free p-HSP20, Figure 4B). Intracellular retention of bioactive cargo can be improved by reducing exocytosis of the intact peptide and/or reducing degradation of the peptide in acidic endo-lysosomal compartments.[18,34] These optimized NP

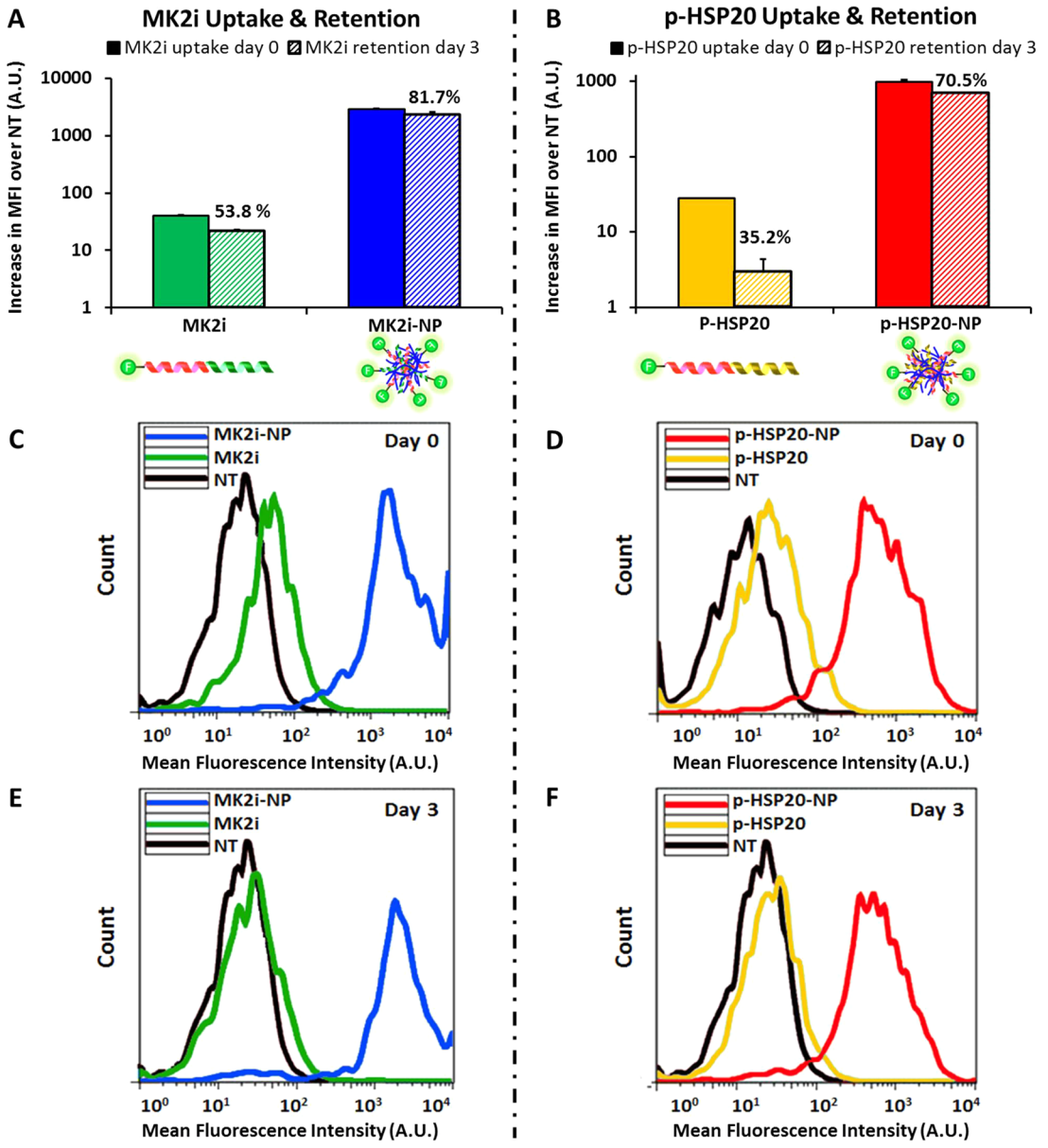

Figure 4. NP uptake and retention. Flow cytometric quantification of peptide uptake and retention of (A) MK2i-NPs *vs* MK2i and (B) p-HSP20-NPs *vs* HSP20 at a 10 μM dose of peptide after 30 min of treatment. MK2i-NPs achieved ~70-fold increase in peptide uptake at the same concentration, whereas p-HSP20-NPs achieved a ~35-fold increase in uptake. (C,D) Representative flow histograms of HCAVSMCs immediately after treatment and (E,F) representative flow histograms demonstrating that formulation into NPs increased peptide cellular retention after 3 days of culture in fresh medium post-treatment. The percentages overwritten on A,B represent the % retention at 3 days relative to 0 days post-treatment.

formulations are intentionally designed to respond to the decreased pH encountered in the endolysosomal trafficking pathway to facilitate cytosolic peptide delivery, as the PPAA polymer has well-defined pH-dependent endosomolytic activity,[35,36] has previously demonstrated biocompatibility in animal models,[37] and has been applied for intracellular delivery of a pro-apoptotic anticancer peptide *via* a multistep bioconjugation of the PPAA polymer to the peptide through a streptavidin linker.[38] Thus, a simplified electrostatic complexation approach was utilized that incorporated the PPAA polymer to facilitate therapeutic endosome escape and retention in these studies: PPAA undergoes a transition from an ionized, expanded conformation at physiologic pH to a collapsed, hydrophobic globular conformation in acidic/endosomal conditions. This transition results in hydrophobic interactions with lipids in the endosomal membrane and ultimately in endosomal escape and improved intracellular retention and bioactivity of the therapeutic peptide cargo.

To investigate the connection between increased peptide intracellular retention and endosomal escape of peptides delivered *via* the NP formulation, a digitonin-based semipermeabilization technique[39] was adapted and optimized for measuring the relative

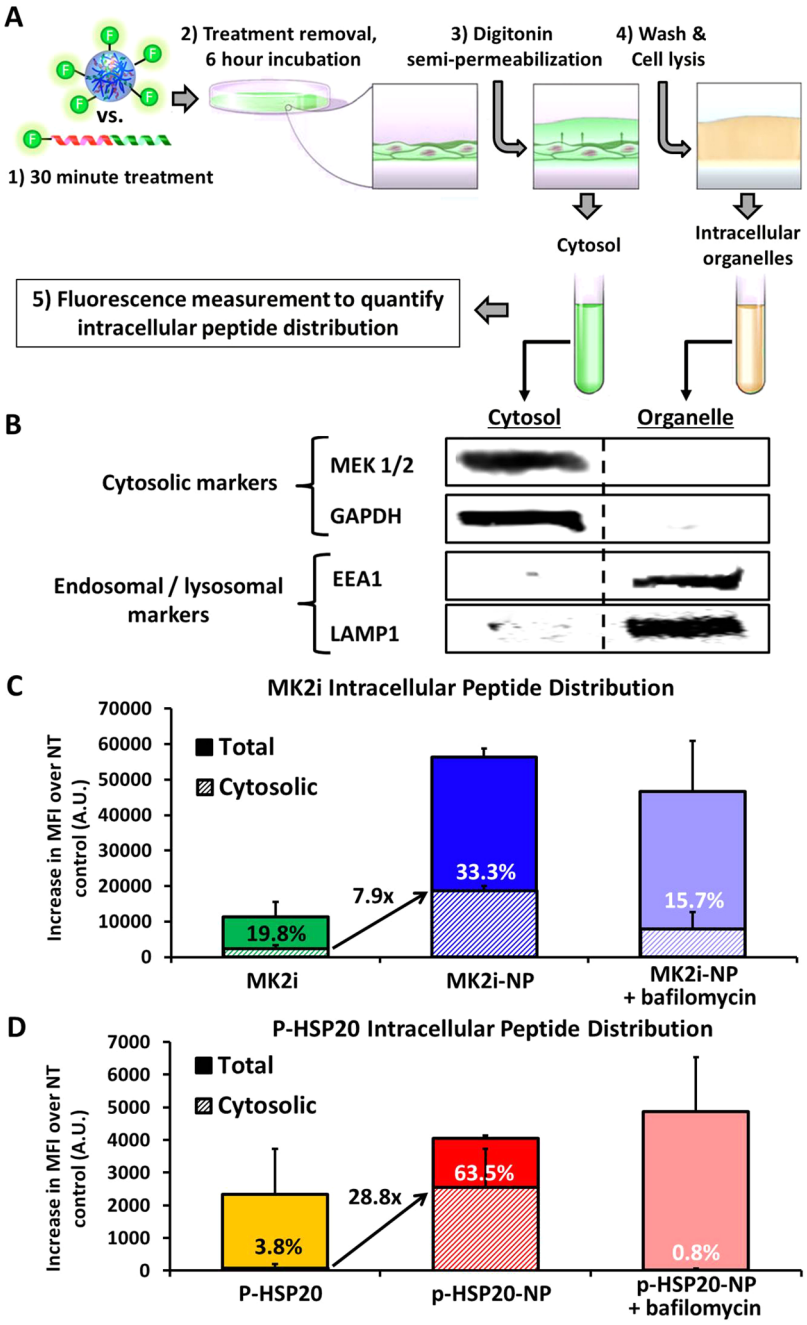

Figure 5. NP endosomal escape and cytosolic peptide delivery. (A) Experimental design for separation of vascular smooth muscle cell cytosol and intracellular organelles using digitonin semipermeabilization. Conditions for semipermeabilization were optimized as shown in Supporting Information Figure S3. (B) Western blot validation of the optimized digitonin semipermeabilization procedure confirmed separation of the cytosolic proteins mitogen-activated protein kinase kinase 1/2 (MEK1/2) and glyceraldehyde 3-phosphate dehydrogenase (GAPDH) from the endolysosomal markers early endosomal antigen 1 (EEA1) and lysosomal-associated protein 1 (LAMP1). Comparison of the intracellular distribution of (C) MK2i and (D) p-HSP20 peptides when delivered alone or formulated into nano-polyplexes, demonstrating increased cytosolic delivery of the NP formulations. Significant inhibition of NP-mediated cytosolic peptide delivery when the endosomal acidification inhibitor bafilomycin was added verified the pH-dependent endosomal escape mechanism of the NPs.

quantity of cytosolic and vesicle-bound peptide for NP and free-peptide-treated HCAVSMCs (Figure 5A). Digitonin is a nonionic detergent that, under optimized conditions, selectively permeabilizes the cell membrane while leaving intracellular organelles (*e.g.*, endosomes and lysosomes) intact. An optimized semipermeabilization procedure was determined by measuring the lactate dehydrogenase (LDH) (which is known to be localized to the cytosol) quantity in the "cytosolic" and "organelle" fractions from HCAVSMCs incubated with a range of concentrations of digitonin for 10 min on ice (Supporting Information Figure S3). Western blot analysis of the cytosolic and organelle fractions collected using the optimized

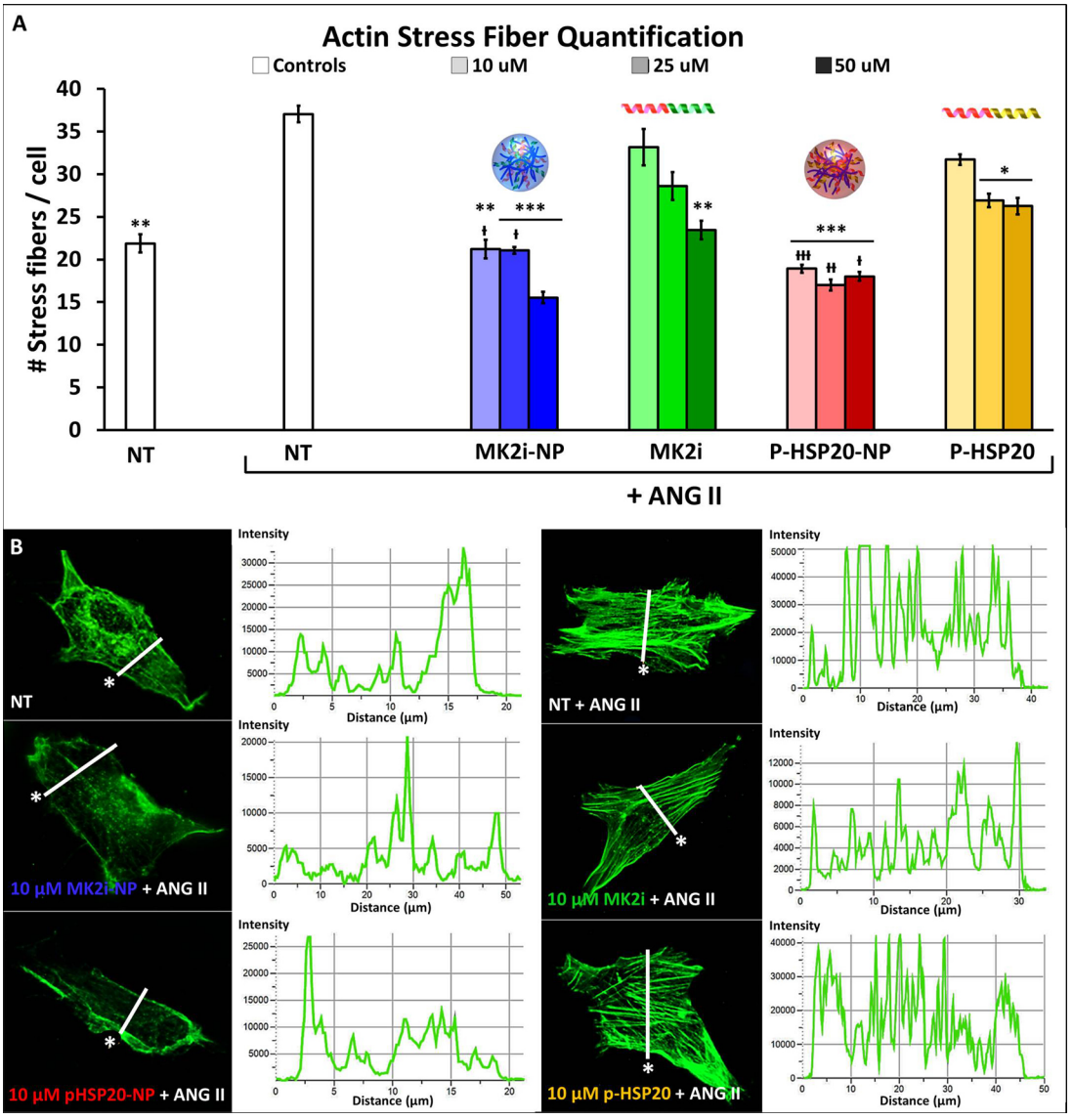

Figure 6. Inhibition of F-actin stress fiber formation in vascular smooth muscle cells. (A) F-actin stress fiber quantification in HCAVSMCs pretreated with p-HSP20-NPs, free p-HSP20 peptide, MK2i-NPs, or free MK2i for 1 h and then stimulated with ANG II for 2 h. The number of stress fibers per cell was calculated from three intensity profiles taken from the axis transverse to the cellular polarity from $n \geq 36$ ROIs from $n \geq 12$ different cells for each treatment group, $^{*}p < 0.05$, $^{**}p < 0.01$, $^{***}p < 0.001$ *vs* NT + ANG II; $^{+}p < 0.1$, $^{++}p < 0.01$, $^{+++}p < 0.001$ *vs* the free peptide at the same concentration. (B) Representative fluorescence microscopy images of F-actin stress fiber formation in ANG II-stimulated HCAVSMCs and the corresponding intensity profile derived from the line shown in the image. The asterisk denotes the left side of the intensity profile shown. Gain settings were kept constant for all images obtained.

semipermeabilization protocol verified effective separation of the cytosolic proteins mitogen-activated protein kinase kinase 1/2 (MEK1/2) and glyceraldehyde 3-phosphate dehydrogenase (GAPDH) from the endolysosomal markers early endosomal antigen 1 (EEA1) and lysosomal-associated protein 1 (LAMP1, Figure 5B). Utilizing fluorescently labeled MK2i and p-HSP20 peptides allowed for quantification of the intracellular distribution of both peptides following delivery in their free form *versus via* NP formulations. This analysis verified that formulation into NPs not only increased peptide uptake but also significantly increased the fraction of internalized peptide in the cytosol; the net effect was an approximately 8-fold increase in cytosolic MK2i delivery and ~29-fold increase in cytosolic p-HSP20 delivery (Figure 5C,D). In order to confirm that the increased cytosolic peptide delivery was facilitated by the pH-dependent membrane disruptive activity of PPAA in the NP formulations, cells were treated with NPs in the presence of the vacuolar-type H^{+} ATPase inhibitor bafilomycin A1 to prevent endolysosomal acidification. Preventing endosomal acidification markedly reduced the fraction of internalized peptide in the cytosol for both NP formulations, confirming that the mechanism of NP escape from edosomes is pH-dependent (Figure 5C,D).

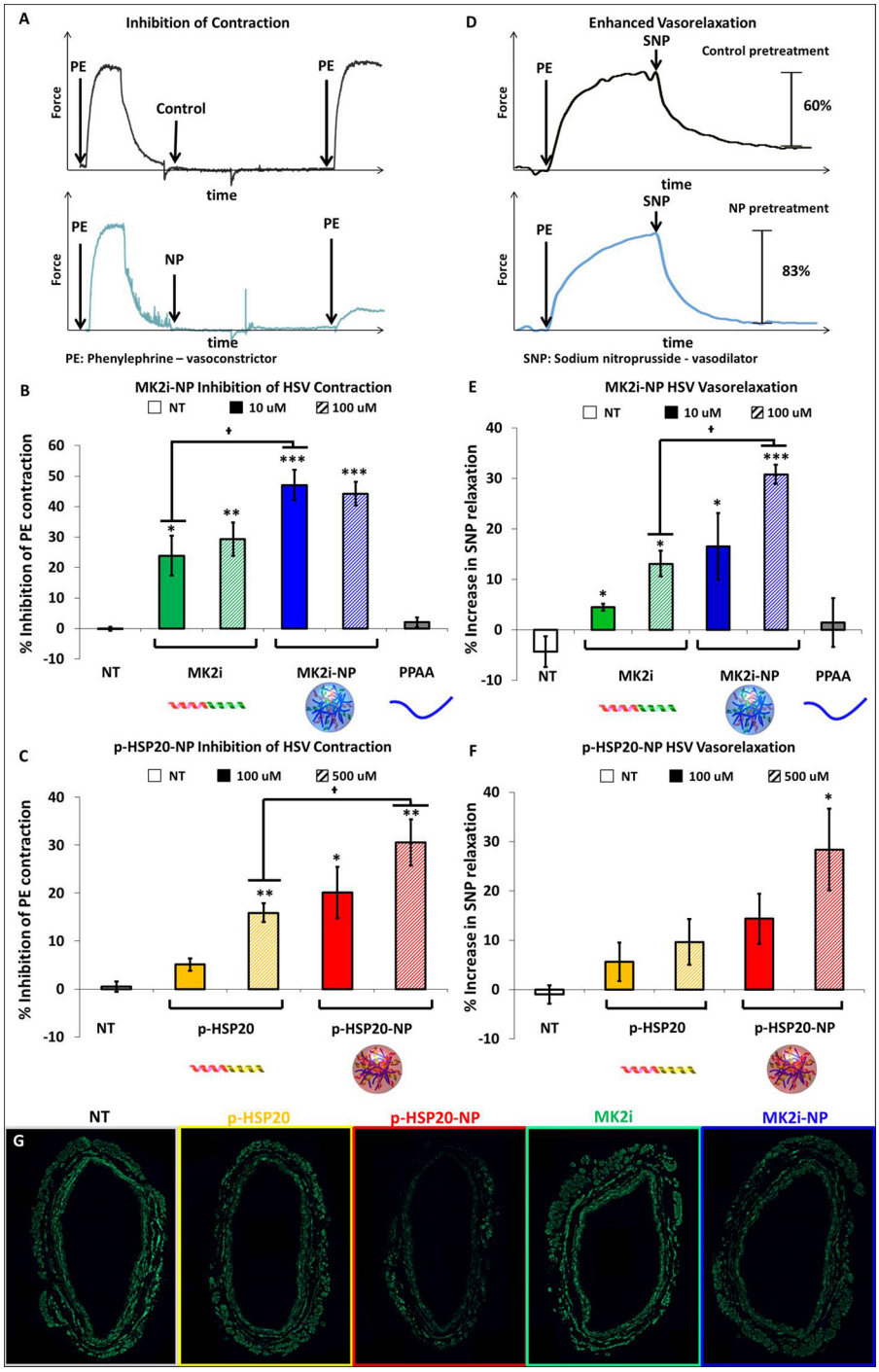

Figure 7. MK2i-NP and p-HSP20-NP treatment inhibits vasoconstriction and enhances vasorelaxation. (A) Experimental design for inhibition of contraction studies: HSV rings are initially contracted with PE and then relaxed. After 2 h of treatment with NPs, free peptide, or control, post-treatment contraction is measured. (B) Quantification of MK2i- and MK2i-NP-mediated inhibition of contraction. PPAA polymer equivalent to the highest dose of MK2i-NPs was included as a vehicle control. (C) Quantification of p-HSP20- and p-HSP20-NP-mediated inhibition of contraction. (D) Experimental design for vasorelaxation studies: HSV rings are initially contracted with PE and subsequently relaxed with sodium nitroprusside. HSV rings are then treated for 2 h with NPs, free peptide, or control and then contracted and relaxed under the same conditions to compare post-treatment to pretreatment relaxation. (E) Quantification of MK2i- and MK2i-NP-enhanced vasorelaxation. PPAA polymer equivalent to the highest dose of MK2i-NPs was included as a vehicle control. (F) Quantification of p-HSP20- and p-HSP20-NP- enhanced vasorelaxation. For B,C,E,F: $^{+}p < 0.05$; *$p < 0.05$, **$p < 0.01$, ***$p < 0.01$ *vs* NT, $n \geq 3$ separate donors. (G) F-actin visualization in Alexa-488 phalloidin stained cryosections of human saphenous vein explants obtained from a single donor ($n = 1$) pretreated with 100 μM MK2i or MK2i-NPs, 500 μM p-HSP20 or p-HSP20-NPs, and subsequently stimulated with ANG II, enabling visualization of decreased F-actin in samples treated with the NP formulations.

Bafilomycin treatment was found to have negligible effects on the cytosolic fraction of internalized free MK2i or p-HSP20 peptide (data not shown; MK2i, 9.64% ± 8.17% cytosolic; p-HSP20, 7.36% ± 8.28% cytosolic).

Subsequently, the efficacy of MK2i-NP- and p-HSP20-NP-mediated inhibition of F-actin stress fiber formation was quantified in angiotensin II (ANG II)-stimulated HCAVSMCs. Both NP formulations enhanced peptide functional bioactivity as measured by a significant decrease in the average number of stress fibers per cell (Figure 6A). Qualitatively, HCAVSMCs treated with the NP formulations and ANG II displayed cell morphology and staining consistent with unstimulated control cells, whereas HCAVSMCs treated with the free peptide demonstrated stress fiber formation similar to ANG II-stimulated control cells (Figure 6B). The total amount of F-actin per cell was also quantified using Alexa-488 phalloidin, a stain that selectively binds to filamentous, but not globular, actin (Supporting Information Figures S4 and S5). This analysis was consistent with the quantification of number of stress fibers per cell and revealed that formulation into NPs significantly enhanced stress fiber inhibitory activity of both peptides.

NP Effect on Smooth Muscle Physiology in Human Vascular Tissue. The effect of the MK2i-NP and p-HSP20-NP formulations on smooth muscle physiology in human vascular tissue was assessed in order to evaluate them as potential treatments for vasospasm. For these studies, human saphenous vein (HSV) was collected from consenting patients undergoing bypass grafting surgery and sectioned into rings. After viability was verified through KCl challenge in a muscle bath, the ability of each NP formulation to inhibit phenylephrine (PE)-induced vasoconstriction was measured in HSV rings using an organ bath system outfitted with a force transducer. In an experimental design where vessels were contracted, relaxed, treated, and then contracted again, untreated control HSV rings displayed no changes in the second round of PE-induced contraction relative to the initial contraction. However, intermediate treatment with the MK2i or p-HSP20 peptides significantly inhibited the second PE-induced HSV contraction (Figure 7A–C). Consistent with *in vitro* F-actin stress fiber results, equivalent doses of peptide delivered *via* NP formulations demonstrated significantly enhanced peptide-mediated inhibition of contraction compared to the free peptide (Figure 7C). Notably, treatment with a dose of free PPAA polymer equivalent to the highest NP dose administered showed negligible effects on PE-induced HSV contraction (Figure 7B), indicating that the enhanced inhibitory activity is mediated through enhancement of peptide bioactivity and is not a nonspecific effect of the endosomolytic polymer carrier. This ability of the peptide NPs to potently inhibit vasoconstriction demonstrates the translational potential of these formulations as a prophylactic approach to prevent vasospasm in applications such as coronary or peripheral bypass grafting.

In addition to testing the efficacy of these NP formulations as a prophylactic therapy, the ability of the MK2i- and p-HSP20-NPs to enhance sodium nitroprusside (SNP)-induced vasorelaxation was evaluated as a potential salutary therapeutic intervention (*e.g.*, to treat SAH-induced vasospasm) in viable HSV explants (Figure 7D). Again, both NP formulations demonstrated an enhanced ability to promote SNP-induced vasorelaxation at all concentrations tested (Figure 7E,F), whereas untreated HSV or HSV treated with the PPAA polymer alone showed negligible differences in vasorelaxation (Figure 7E). Because MK2i-NP and p-HSP20-NP formulations trigger vasorelaxation through separate molecular mechanisms, combining both peptides into a NP formulation represents a promising approach for future studies because it may achieve a synergistic effect that produces a therapeutic benefit at lower peptide doses.

In order to qualitatively assess the correlation of F-actin stress fiber formation with the smooth muscle physiology results in human tissue, HSV rings were pretreated with free peptide or the NP formulations and then subsequently stimulated with ANG II prior to F-actin staining with Alexa-488 phalloidin (Figure 7G). In concordance with the smooth muscle physiology results, HSV rings treated with NP formulations showed diminished phalloidin staining compared to HSV treated with the free peptide. Altogether, these results indicate that MK2i- and p-HSP20-NPs significantly enhance the ability of the MK2i and p-HSP20 peptides to inhibit vasoconstriction and promote vasorelaxation by modulating actin dynamics in human smooth muscle tissue.

CONCLUSION

A platform technology was developed for formulation of electrostatically complexed nanoparticles that facilitate intracellular delivery, endosomal escape, and bioactivity of therapeutic peptides. Specifically, this platform was applied to deliver vasoactive peptides that modulate smooth muscle physiology by affecting actin dynamics. NP formulation enhanced the potency of both a MK2 inhibitory peptide and a phosphorylated HSP20 mimetic peptide, and the translatability of this delivery technology was demonstrated in human vascular tissue *ex vivo*. These results also validate and provide mechanistic insight into the role of actin dynamics in vascular smooth muscle physiology and highlight promising therapeutic targets for prevention of pathological vasoconstriction and enhancement of salutary vasorelaxation. However, for future translation of this approach *in vivo*, additional nano-polyplex design considerations may be required to enable effective intravenous or cisternal (*i.e.*, suboccipital puncture) administration. For example, cross-linking the nanopolyplex or incorporating surface-shielding polymers such as poly(ethylene glycol) may be required for increasing blood and/or CSF stability and circulatory half-life, respectively. There is also potential for

endowing nano-polyplexes with tissue- or cell-specific targeting through receptor ligand or antibody conjugation to the polymeric carrier,[40] fusion of the therapeutic peptide with targeting peptide sequences,[41] or incorporation of enzyme-removable surface PEGylation.[42]

This nano-polyplex platform is potentially more broadly applicable for therapeutic peptide delivery. The most common approach to increasing therapeutic peptide uptake and bioactivity is fusion with a cell-penetrating peptide (CPP) sequence that is positively charged (*e.g.*, polyarginine, polylysine, trans-activator of transcription or TAT, penetratin, *etc.*) in order to facilitate electrostatic interactions with the cell surface.[43−45] For example, the MK2i and p-HSP20 parent peptides used in this study both contain a CPP sequence that is a modified form of the HIV-derived TAT peptide (*i.e.*, YARAAARQARA). However, despite improving cellular uptake, many CPPs do not address the key delivery barrier of endosomal entrapment[8] and their potency suffers as a result. Since most therapeutic peptides include a cationic CPP sequence, the electrostatic polyplex approach demonstrated here is widely applicable for enhancement of therapeutic peptide delivery by facilitating increased uptake and endolysosomal escape. This approach is also desirable because simple mixing of a cationic therapeutic peptide with an anionic endosomolytic agent represents a simple, cost-effective strategy to enhance the efficacy of peptides that avoids complex and costly synthesis schemes that are associated with many colloidal drug delivery carriers.[46] Furthermore, the global pharmaceutical industry has faced prohibitive costs in the development of new molecular entities; thus, the nano-polyplex technology presented herein befits the major transition that is occurring to shift focus onto the development of drug delivery systems that can improve extant therapeutics.[47]

MATERIALS AND METHODS

MAPKAP Kinase II Inhibitor Peptide and Phosphorylated Heat Shock Protein 20 Mimetic Peptide Syntheses. A cell-permeant MK2 inhibitory peptide with the sequence YARAAARQARA-KALARQLGVAA and a cell-permeant phosphorylated heat shock protein 20 mimetic peptide with the sequence YARAAARQARA-WLRRAsAPLPGLK (where s denotes a phosphorylated serine residue corresponding to serine 16 in HSP20 that is activated by cyclic nucleotide signaling) were synthesized on a PS3 peptide synthesizer (Protein Technologies, Inc., Tucson, AZ) utilizing standard Fmoc chemistry. *N*-Methylpyrrolidone (Fischer Scientific) was utilized as a solvent in all peptide syntheses. HCTU was used as an activator (Chempep, Wellington, FL) in the presence of *N*-methylmorpholine. All amino acids were double coupled in order to maximize yield and purity. Peptides were cleaved/deprotected in trifluoroacetic acid/phenol/H_2O/triisopropylsilane (88/5/5/2). The peptide was then further purified by reversed-phase high-performance liquid chromatography (HPLC) on a Waters 1525 binary HPLC pump outfitted with an extended flow kit, a Waters 2489 UV/visible detector, and a Phenomenex Luna C18(2) AXIA packed column (100 A, 250 × 21.2 mm, 5 μm). (A) HPLC-grade water with 0.05% formic acid and (B) HPLC-grade acetonitrile were used as the mobile phase, and the peptide was purified utilizing a 90% A to 90% B gradient over 25 min (16 mL/min). Acetonitrile was removed from purified fractions with a rotary evaporator, and the purified fractions were then lyophilized. Peptide purity was verified through analysis on a Waters Synapt ESI-MS.

Monomer and Polymer Synthesis. All reagents were purchased from Sigma and were of analytical grade unless otherwise stated. 2-Propylacrylic acid was synthesized according to the procedure outlined by Ferrito *et al.*[48] utilizing diethyl propylmalonate (Alfa Aesar) as a precursor. The 4-cyano-4-(ethylsulfanylthiocarbonyl) sulfanylpentanoic acid chain transfer agent (CTA) was synthesized as previously described.[49] RAFT polymerization of the poly(propylacrylic acid) was carried out in bulk under a nitrogen atmosphere at 70 °C for 48 h using 2,2′-azobisisobutyrylnitrile (AIBN) as the free radical initiator. The reaction mixture was put through three freeze−vacuum−thaw cycles and purged with nitrogen for 30 min prior to polymerization. The molar ratio of CTA to AIBN was 1:1, and the monomer to CTA ratio was set so that a degree of polymerization of 190 would be achieved at 100% conversion. Following polymerization, the resultant polymer was dissolved in dimethylformamide (DMF) and precipitated into ether five times before being dried overnight *in vacuo*. Gel permeation chromatography (GPC, Agilent) was used to determine molecular weight and polydispersity (M_w/M_n, PDI) of the PPAA homopolymer using HPLC-grade DMF containing 0.1% LiBr at 60 °C as the mobile phase. Molecular weight calculations were performed with ASTRA V software (Wyatt Technology) and were based on experimentally determined d*n*/d*c* values determined through offline injections of serial dilutions of the polymer through a refractive index detector (calculated PPAA d*n*/d*c* = 0.087 mL/g). Polymer purity and molecular weight were then verified through NMR spectroscopy. Samples were dissolved in deuterated dimethyl sulfoxide and analyzed using a Bruker 400 MHz NMR spectrometer equipped with a 9.4 T Oxford magnet controlled by a Bruker VA-400 console. NMR spectra were subsequently analyzed using Bruker Topspin 3.0 software.

MK2i Nano-Polyplex and Phospho-HSP20 Nano-Polyplex Synthesis and Characterization. PPAA was dissolved in 1 M NaOH and diluted into a phosphate buffer (pH 8) to obtain a stock solution. Purified MK2i peptide or p-HSP20 peptide was dissolved in phosphate buffer (pH 8). The MK2i peptide or p-HSP20 peptide was then mixed with the PPAA polymer at a range of CRs from $[NH_3^+]/[COO^-]$ = 10:1 to 1:10 to form MK2i-NPs or p-HSP20-NPs, respectively. The resulting nano-polyplexes were syringe-filtered through a 0.45 μm PTFE (polytetrafluorethylene) filter, and the hydrodynamic diameter and ζ-potential were characterized on a Malvern Zetasizer Nano-ZS with a reusable dip cell kit (Malvern Instruments Ltd., Worcestershire, U.K.).

A CR of 1:3 was chosen as the lead MK2i-NP formulation, whereas a charge ratio of 3:1 was chosen as the lead p-HSP20-NP formulation; these formulations were used in subsequent *in vitro* and *ex vivo* experiments. In order to verify the sizes indicated by DLS analysis, optimized MK2i-NP and HSP20-NP formulations were visualized through transmission electron microscopy imaging. TEM samples were prepared by inverting carbon-film-backed copper grids (Ted Pella) onto a 20 μL droplet of aqueous polyplex suspensions (1 mg/mL) and blotted dry. All samples were then inverted onto a 20 μL droplet of 3% uranyl acetate and stained for 30 s. Samples were then desiccated *in vacuo* for 2 h prior to imaging on a FEI Tecnai Osiris system.

Cell Culture. Primary human coronary artery vascular smooth muscle cells were obtained from Lonza; HCAVSMCs were cultured in complete growth medium [vascular cell basal medium (ATCC) supplemented with 5% fetal bovine serum (FBS), human basic fibroblast growth factor (5 ng/mL), human

insulin (5 μg/mL), ascorbic acid (50 μg/mL), L-glutamine (10 mM), human epidermal growth factor (5 ng/mL), 1% penicillin−streptomycin and 50 μg/mL plasmocin (Invivogen)] in a sterile incubator maintained at 37 °C with a humidified 5% CO_2 atmosphere.

All cultures were maintained in 75 cm^2 polystyrene tissue culture flasks (BD Falcon) in a 37 °C and 5% CO_2 environment with cell culture media refreshed every other day. Cells were grown to 80−90% confluence prior to being harvested and passaged. All cells were seeded at a density of 20000−30000 cells/cm^2, as required for each specific experiment. Only cells from early passages (numbers 3−8) were used in experiments.

Cytotoxicity Assay. A cell suspension (200 μL at 10000 cells/well) was seeded onto 96-well plates to yield an approximate 70% confluence per well. Cells were allowed to adhere to the plate overnight. Cells were then treated with 10, 50, 100, and 500 μM doses of MK2i-NPs, p-HSP20-NPs, MK2i peptide, p-HSP20 peptide, or PBS as a control treatment for 2 h in Opti-MEM medium supplemented with 1% penicillin−streptomycin. Treatments were subsequently removed, and the cells were cultured in fresh complete growth medium for 24 h. Cells were then washed twice with PBS +/+, and cell viability was then determined by a CytoTox-ONE homogenous membrane integrity assay (Promega) according to the manufacturer's protocol. Briefly, 100 μL of Ambion KDalert lysis buffer was added to each well, and then 100 μL of freshly prepared CytoTox-ONE reagent was added to each well. After 10 min of incubation, 50 μL of stop solution was added, and the fluorescence of each well (λ_{ex} = 560 nm, λ_{em} = 590 nm) was determined with a TECAN Infinite M1000 Pro plate reader.

Flow Cytometric Quantification of Peptide Uptake and Retention in HCAVSMCs. An amine-reactive Alexa-488 succinimidyl ester (Life Technologies) was dissolved in dimethylsulfoxide and mixed at a 1:3 molar ratio with the MK2i or p-HSP20 peptide in 100 mM sodium bicarbonate buffer (pH = 8.3) and allowed to react for 3 h. Unreacted fluorophore and organic solvent were removed using a PD-10 miditrap G-10 desalting column, and the fluorescently labeled MK2i and p-HSP20 peptides were lyophilized. PPAA polymer was mixed with fluorescently labeled MK2i peptide at a CR of $[NH_3^+]/[COO^-]$ = 1:3 and syringe-filtered through a 0.45 μm PTFE filter to form fluorescent MK2i-NPs. Similarly, PPAA was mixed with fluorescently labeled p-HSP20 at a CR of $[NH_3^+]/[COO^-]$ = 1:3 and syringe-filtered through a 0.45 μm PTFE filter to form fluorescent HSP20-NPs. HCAVSMCs were grown to 80−90% confluence, harvested, and seeded at 20000 cells/well in a 24-well plate and allowed to adhere overnight. HCAVSMCs were treated with fluorescent MK2i peptide, MK2i-NPs, p-HSP20 peptide, p-HSP20-NPs, or PBS as a control at a concentration of 10 μM peptide in Opti-MEM medium supplemented with 1% penicillin−streptomycin for 30 min. Following treatment, cells were washed twice in PBS and either immediately harvested or incubated in complete growth media for an additional 72 h. Cells were harvested with 0.05% trypsin-EDTA, centrifuged, and suspended in 0.1% Trypan blue in PBS (−/−) for analysis on a FACSCalibur flow cytometer (Becton Dickinson) with BD CellQuest Pro software (V 5.2). Data were exported and analyzed with FlowJo software (V 7.6.4). All samples were run in triplicate.

F-Actin Stress Fiber Assay. HCAVSMCs were seeded in Lab-Tek II 8-well chambered coverglass (Thermo Scientific Nunc) at 15000 cells/well and allowed to adhere overnight. Cells were then treated in low serum media (Optimem, 1% FBS, and 1% P/S) with MK2i-NPs, p-HSP20-NPs, MK2i peptide, or p-HSP20 peptide or at concentrations of 10, 25, and 50 μM (PBS −/− as a control) for 1 h. Following treatment, cells were washed twice with PBS −/− and subsequently treated with 1 μM angiotensin II (Sigma-Aldrich) or PBS −/− (negative control) for 2 h. Afterward, ANG II stimulation cells were washed twice with PBS, fixed in 4% paraformaldehyde for 5 min, permeabilized with 0.4% Triton-X 100 for 10 min, and blocked with 1% BSA in PBS −/− for 15 min. Cells were then stained with Hoechst solution (1/5000 dilution in PBS −/−) for 10 min followed by staining with Alexa-488 phalloidin (Life Technologies) for 30 min according to the manufacturer's instructions. Stained coverslips were then inverted onto glass cover slides with ProLong gold antifade mounting medium (Invitrogen). Slides were allowed to dry for 24 h prior to sealing and imaging. Treated cells were imaged using a Nikon Eclipse Ti inverted fluorescence microscope (Nikon Instruments Inc., Melville, NY) with NIS Elements imaging software. Gain settings and exposure times were kept constant for all images taken. The number of stress fibers per cell was quantified as previously described.[50] Briefly, in the NIS elements software, three separate intensity profiles were generated across the axis of stained cells perpendicular to the cell's polarity. Prior to image analysis, the background noise from each image was removed using a rolling ball background subtraction filter with a radius of 70 pixels. A fluorescence level of 2000 rfu was set as the threshold for positive F-actin fiber staining as the background fluorescence outside of the stained cells was never greater than this value. The stress fibers per cell were then quantified from the average of three intensity profiles from $n \geq 6$ cells from two separate experiments for each treatment group (total $n \geq 36$ ROIs for each treatment group). Relative quantification of cellular F-actin content was further quantified using ImageJ software to free hand select individual cells and to calculate the relative fluorescence intensity of $n \geq 12$ cells from two separate experiments for each treatment group.

Quantification of Cytosolic *versus* Organelle-Bound Peptide through Semipermeabilization. In order to quantify the cytosolic bioavailability of the MK2i and HSP20 peptides, a method to separate cytosolic and organelle-bound (*i.e.*, endosomal, lysosomal, golgi, *etc.*) peptide was adapted from the methods developed by Liu *et al.*[39] The procedure was optimized for this experiment based upon LDH release from HCAVSMCs treated with varying concentrations of digitonin (Calbiochem) in buffer (150 mM NaCl, 0.2 mM EDTA, 20 mM HEPES/NaOH (pH 7.4), 2 mM DTT, and 2 mM $MgCL_2$) on ice for 10 min on a rotary shaker operating at 100 rpm (Supporting Information Figure S3). A concentration of 25 μg/mL was then chosen as the optimal digitonin concentration for selective semipermeabilization of the HCAVSMC membrane and subsequently used for the analysis of intracellular peptide distribution.

To quantify intracellular distribution of the MK2i and p-HSP20 peptides, HCAVSMCs were seeded into a 96-well plate at a density of 20000 cells/cm^2 and allowed to adhere overnight in complete growth medium. A portion of the cells was pretreated with 500 nM bafilomycin A1 (Sigma) for 30 min, and the bafilomycin was included in subsequent peptide/NP treatment and in the post-treatment incubation phase to inhibit endosomal acidification. Cells were then treated with Alexa-488-labeled MK2i peptide, MK2i-NPs, p-HSP20 peptide, and p-HSP20-NPs at a concentration of 10 μM peptide (or PBS −/− as a control) in Opti-MEM medium supplemented with 1% penicillin−streptomycin with or without 500 nM bafilomycin A1 for 30 min. Treatments were removed, and cells were incubated in fresh medium with or without 500 nM bafilomycin A1 for 6 h. Each well was then washed once with ice-cold PBS +/+ and then subsequently incubated with 20 μL of 25 μg/mL digitonin solution at 0 °C (on ice) on a rotary shaker operating at 100 rpm for 10 min. The supernatant from each well was then transferred to a new 96-well plate, and each well was washed with 80 μL of ice-cold PBS +/+, which was then transferred to the 96-well plate containing the digitonin (cytosolic) fractions. One hundred microliters of 1% Triton X-100 in PBS −/− was then added to each well to obtain a 96-well plate containing all noncytosolic (*i.e.*, organelle-bound) cellular components, and the fluorescence of each well (λ_{ex} = 495 nm, λ_{em} = 519 nm) was determined with a TECAN Infinite M1000 Pro plate reader. Readings were normalized to cell number and cytosolic content as determined by a CytoTox-ONE homogenous membrane integrity assay (Promega) according to the manufacturer's protocol (Cytotoxicity Assay section).

Western Blot Verification of Cytosolic Separation from Intracellular Organelles. To further verify separation of the cytosol from intracellular organelles such as endosomes and lysosomes, Western blot analysis of the cytosolic and organelle fractions from the digitonin semipermeabilization procedure was performed. Briefly, cytosolic and organelle fractions were concentrated on a centrifuge using Vivacon 500 DNA concentrators

(2000 MWCO). Equal amounts of protein (20 μg per lane) were loaded on 4−20% SDS−PAGE gels; proteins were electrophoretically separated and then transferred to Immobilon membranes. The membranes were then probed overnight at 4 °C with primary antibodies for the cytosolic proteins mitogen-activated protein kinase kinase 1/2 and glyceraldehyde 3-phosphate dehydrogenase and the endolysosomal markers early endosomal antigen 1 and lysosomal-associated protein 1. All antibodies were obtained from Cell Signaling Technologies. After being washed, the membranes were incubated with appropriate secondary antibodies (Li-Cor) for 1 h at room temperature. The secondary antibody was imaged using the Odyssey direct infrared fluorescence imaging system and densitometrically quantified with LiCor Odyssey software v2.1 at 800 and 680 nm wavelengths.

Human Saphenous Vein. Upon approval by Vanderbilt Medical Center's Institutional Review Board, deidentified, discarded segments of HSV were collected from consenting patients undergoing coronary or peripheral vascular bypass surgeries. Following surgical resection, HSV segments were stored in buffered salt solution until the end of the surgical procedure, at which time they were placed in cold transplant harvest buffer (100 mM potassium lactobionate, 25 mM KH_2PO_4, 5 mM $MgSO_4$, 30 mM raffinose, 5 mM adenosine, 3 mM glutathione, 1 mM allopurinol, 50 g/L hydroxyethyl starch, pH 7.4). All HSV segments were used within 24 h of harvest. Utilizing sterile technique in a sterile culture hood, we transferred HSV segments to a 60 mm Petri dish. The end of each segment (0.5 mm) was removed with a blade, and excess adventitial and adipose tissue was removed with minimal manipulation. HSV segments were cut into consecutive rings with an approximate width of 1.0 mm.

Prior to experiments, HSV viability was confirmed. HSV rings were weighed and their lengths recorded. HSV rings were then suspended in a muscle bath containing a bicarbonate buffer (120 mM NaCl, 4.7 mM KCl, 1.0 mM $MgSO_4$, 1.0 mM NaH_2PO_4, 10 mM glucose, 1.5 mM $CaCl_2$, and 25 mM Na_2HCO_3, pH 7.4) equilibrated with 95% O_2 and 5% CO_2 at 37 °C. The rings were stretched, and the length was progressively adjusted until maximal tension was obtained.[51] Normalized reactivity was obtained by determining the passive length−tension relationship for each vessel segment. Rings were maintained at a resting tension of 1 g, which produces maximal responses to contractile agonists, as previously determined, and equilibrated for 2 h in buffer. Force measurements were obtained using a Radnoti Glass Technology (Monrovia, CA) force transducer (159901A) interfaced with a Powerlab data acquisition system and LabChart software (AD Instruments, Colorado Springs, CO).

HSV rings were initially isometrically contracted with 110 mM KCl (with equimolar replacement of NaCl in bicarbonate buffer), and the generated force was measured. The 110 mM KCl causes membrane depolarization, leading to contraction of vessels containing functionally viable smooth muscle. After vessel viability was verified with multiple KCl challenges, additional rings were cut to be utilized in smooth muscle physiology experiments and for F-actin staining.

HSV Smooth Muscle Physiology Studies. *Inhibition of HSV Contraction.* Viable HSV rings were washed, allowed to equilibrate in bicarbonate solution for 30 min, and then contracted with phenylephrine (1 μM). All rings were washed and equilibrated in fresh buffer and allowed to relax until baseline contraction was achieved. Rings were then incubated with either MK2i peptide, MK2i-NPs, p-HSP20 peptide, p-HSP20-NPs, or buffer alone for 2 h. Treated HSV rings were then contracted with the same doses of PE, and the forces generated were again recorded (see Figure 7A). Measured force was normalized for ring weight and length, and percent inhibition of contraction was calculated by dividing the post-treatment contractile force with the pretreatment contractile force; pretreatment force generated with 1 μM PE was set as 100% contraction. Data were obtained in HSV from $n \geq 3$ separate patients.

Enhanced HSV Vasorelaxation. Viable HSV rings were washed and allowed to equilibrate in bicarbonate solution for 30 min and then contracted with phenylephrine (1 μM). Rings were relaxed with a cumulative log dose of sodium nitroprusside (0.1−10 μM), a nitric oxide donor, and the resulting decrease in contractile force was recorded over time (see Figure 7D). All rings were again washed and equilibrated in buffer for 15 min. Rings were then incubated with either MK2i peptide, MK2i-NPs, p-HSP20, p-HSP20-NPs, or buffer alone for 2 h, followed by treatment with the same doses of PE and SNP. The forces generated were again recorded, and measured force was normalized for ring weight and length, and percent relaxation was calculated; force generated with 100 μM PE was set as 0% relaxation. Data were obtained in HSV from $n \geq 3$ separate patients.

Actin Staining of Angiotensin II-Stimulated HSV. Viable HSV rings were placed in a 24-well plate in RPMI medium supplemented with 10% FBS and 1% penicillin−streptomycin and allowed to equilibrate in an incubator at 37 °C and 5% CO_2 for several hours. HSV rings were then treated with 100 μM MK2i peptide, 100 μM MK2i-NPs, 500 μM p-HSP20, or 500 μM p-HSP20-NPs or PBS −/− as a negative control for 30 min in Opti-MEM medium supplemented with 1% penicillin−streptomycin and then washed twice in PBS −/−. Subsequently, treated HSV rings were stimulated with 10 μM angiotensin II for 2 h and then washed twice in PBS −/−. HSV rings were then immediately fixed in 4% paraformaldehyde for 4 h at 37 °C. HSV rings were then incubated overnight in 30% sucrose in 1× PBS −/−. HSV rings were washed twice in PBS −/−, embedded in OCT, and frozen. Ten micrometer cryosections were cut from the midportion of each HSV ring and placed onto SuperFrost Plus microscope slides (Fisher Scientific). The slides were then stained and imaged according to the procedure stated in the F-Actin Stress Fiber Assay section. Full HSV sections were compiled through the image stitching capability in the NIS Elements software.

Statistics. Statistical analysis was performed with one-way ANOVA followed by Tukey's posthoc test to compare experimental groups. Analyses were done with OriginPro 8 software (Originlab, Northampton, MA) or Minitab 16 software (State College, PA). Statistical significance was accepted within a 95% confidence limit. Results are presented as arithmetic mean ± SEM graphically, and p values are included within figures or in the figure captions.

Conflict of Interest: The authors declare the following competing financial interest(s): C.M.B. is a stockholder/consultant to Morae Matrix, Inc.

Acknowledgment. Confocal imaging was performed in part through the use of the VUMC Cell Imaging Shared Resource (supported by NIH Grants CA68485, DK20593, DK58404, HD15052, DK59637, and Ey008126). DLS and TEM were conducted at the Vanderbilt Institute of Nanoscale Sciences and Engineering (VINSE). Histological sectioning and immunostaining were performed in part by the Vanderbilt Translational Pathology Shared Resource (TPSR). This work was supported by AHA 11SDG4890030, NIH 1R21HL110056-01, and a National Science Foundation Graduate Research Fellowship to B.C.E. (DGE-0909667). The authors thank Alyssa Panitch, Joyce-Cheung Flynn, and Padmini Komalavilas for their input on experimental study design. C.L.D. and C.M.B. conceived and directed the project. B.C.E. synthesized, formulated, and characterized NPs and performed *in vitro* assays, flow cytometry, HSV phalloidin staining, image analysis, and statistical analysis. K.M.H. performed smooth muscle physiology and Western blot experiments. K.V.K. performed fluorescence confocal microscopy. E.S.W. obtained patient consent and obtained human tissue samples. B.C.E. wrote the manuscript and received feedback and final approval from all other authors.

Supporting Information Available: Mass spectra of the purified MK2i and p-HSP20 peptides, MK2i-NP and p-HSP20-NP library size distribution analysis tables, cytotoxicity results in HCAVSMCs, digitonin semipermeabilization optimization based on LDH release from HCAVSMCs, and F-actin stress fiber quantification in treated HCAVSMCs based upon relative cellular fluorescence. The Supporting Information is available free of charge on the ACS Publications website at DOI: 10.1021/acsnano.5b00491.

REFERENCES AND NOTES

1. Wilson, T. R.; Johnston, P. G.; Longley, D. B. Anti-apoptotic Mechanisms of Drug Resistance in Cancer. *Curr. Cancer Drug Targets* **2009**, *9*, 307–319.
2. Alexander, J. H.; Hafley, G.; Harrington, R.; Peterson, E. D.; Ferguson, T. B.; Lorenz, T. J.; Goyal, A.; Gibson, M.; Mack, M. J.; Gennevois, D.; et al. Efficacy and Safety of Edifoligide, an E2F Transcription Factor Decoy, for Prevention of Vein Graft Failure Following Coronary Artery Bypass Graft Surgery—PREVENT IV: A Randomized Controlled Trial. *JAMA* **2005**, *294*, 2446–2454.
3. Craik, D. J.; Fairlie, D. P.; Liras, S.; Price, D. The Future of Peptide-Based Drugs. *Chem. Biol. Drug Des.* **2013**, *81*, 136–147.
4. Ewing, M. M.; de Vries, M. R.; Nordzell, M.; Pettersson, K.; de Boer, H. C.; van Zonneveld, A. J.; Frostegard, J.; Jukema, J. W.; Quax, P. H. A. Annexin A5 Therapy Attenuates Vascular Inflammation and Remodeling and Improves Endothelial Function in Mice. *Arterioscler., Thromb., Vasc. Biol.* **2011**, *31*, 95–101.
5. Al-Taei, S.; Penning, N. A.; Simpson, J. C.; Futaki, S.; Takeuchi, T.; Nakase, I.; Jones, A. T. Intracellular Traffic and Fate of Protein Transduction Domains HIV-1 TAT Peptide and Octaarginine. Implications for Their Utilization as Drug Delivery Vectors. *Bioconjugate Chem.* **2006**, *17*, 90–100.
6. Belting, M.; Sandgren, S.; Wittrup, A. Nuclear Delivery of Macromolecules: Barriers and Carriers. *Adv. Drug Delivery Rev.* **2005**, *57*, 505–527.
7. Duvall, C. L.; Convertine, A. J.; Benoit, D. S.; Hoffman, A. S.; Stayton, P. S. Intracellular Delivery of a Proapoptotic Peptide *via* Conjugation to a RAFT Synthesized Endosomolytic Polymer. *Mol. Pharmaceutics* **2010**, *7*, 468–476.
8. Flynn, C. R.; Cheung-Flynn, J.; Smoke, C. C.; Lowry, D.; Roberson, R.; Sheller, M. R.; Brophy, C. M. Internalization and Intracellular Trafficking of a PTD-Conjugated Anti-fibrotic Peptide, AZX100, in Human Dermal Keloid Fibroblasts. *J. Pharm. Sci.* **2010**, *99*, 3100–3121.
9. Chorev, M.; Chaturvedi, N.; Shavitz, R.; Goodman, M. Partially Modified Retro-Inverso-Peptides: Novel Modification of Biologically-Active Peptides. *Fed. Proc.* **1979**, *38*, 363.
10. Taylor, J. W. The Synthesis and Study of Side-Chain Lactam-Bridged Peptides. *Biopolymers* **2002**, *66*, 49–75.
11. Kritzer, J. A. Stapled Peptides: Magic Bullets in Nature's Arsenal. *Nat. Chem. Biol.* **2010**, *6*, 566–567.
12. Cahill, K. Cell-Penetrating Peptides, Electroporation and Drug Delivery. *IET Syst. Biol.* **2010**, *4*, 367–378.
13. De Coupade, C.; Fittipaldi, A.; Chagnas, V.; Michel, M.; Carlier, S.; Tasciott, E.; Darmon, A.; Ravel, D.; Kearsey, J.; Giacca, M.; et al. Novel Human-Derived Cell-Penetrating Peptides for Specific Subcellular Delivery of Therapeutic Biomolecules. *Biochem. J.* **2005**, *390*, 407–418.
14. Efremov, R. G.; Nolde, D. E.; Volynsky, P. E.; Chernyavsky, A. A.; Dubovskii, P. V.; Arseniev, A. S. Factors Important for Fusogenic Activity of Peptides: Molecular Modeling Study of Analogs of Fusion Peptide of Influenza Virus Hemagglutinin. *FEBS Lett.* **1999**, *462*, 205–210.
15. Ayame, H.; Morimoto, N.; Akiyoshi, K. Self-Assembled Cationic Nanogels for Intracellular Protein Delivery. *Bioconjugate Chem.* **2008**, *19*, 882–890.
16. Ko, Y. T.; Falcao, C.; Torchilin, V. P. Cationic Liposomes Loaded with Proapoptotic Peptide D-(KLAKLAK)(2) and Bcl-2 Antisense Oligodeoxynucleotide G3139 for Enhanced Anticancer Therapy. *Mol. Pharmaceutics* **2009**, *6*, 971–977.
17. Yamada, Y.; Akita, H.; Kogure, K.; Kamiya, H.; Harashima, H. Mitochondrial Drug Delivery and Mitochondrial Disease Therapy: An Approach to Liposome-Based Delivery Targeted to Mitochondria. *Mitochondrion* **2007**, *7*, 63–71.
18. Foster, S.; Duvall, C. L.; Crownover, E. F.; Hoffman, A. S.; Stayton, P. S. Intracellular Delivery of a Protein Antigen with an Endosomal-Releasing Polymer Enhances CD8 T-Cell Production and Prophylactic Vaccine Efficacy. *Bioconjugate Chem.* **2010**, *21*, 2205–2212.
19. Baek, J. H.; Han, S. S.; Lee, D. H. Native Coronary Artery and Grafted Artery Spasm Just after Coronary Artery Bypass Grafting: A Case Report. *J. Korean Med. Sci.* **2010**, *25*, 641–643.
20. Lorusso, R.; Crudeli, E.; Luca, F.; De Cicco, G.; Vizzardi, E.; D'Aloia, A.; Gelsomino, S. Refractory Spasm of Coronary Arteries and Grafted Conduits after Isolated Coronary Artery Bypass Surgery. *Ann. Thorac. Surg.* **2012**, *93*, 545–551.
21. Feigin, V. L.; Rinkel, G. J.; Lawes, C. M.; Algra, A.; Bennett, D. A.; van Gijn, J.; Anderson, C. S. Risk Factors for Subarachnoid Hemorrhage: An Updated Systematic Review of Epidemiological Studies. *Stroke* **2005**, *36*, 2773–2780.
22. Van Gijn, J.; Kerr, R. S.; Rinkel, G. J. Subarachnoid Haemorrhage. *Lancet* **2007**, *369*, 306–318.
23. Kassell, N. F.; Peerless, S. J.; Durward, Q. J.; Beck, D. W.; Drake, C. G.; Adams, H. P. Treatment of Ischemic Deficits from Vasospasm with Intravascular Volume Expansion and Induced Arterial Hypertension. *Neurosurgery* **1982**, *11*, 337–343.
24. Chen, H. F.; Xie, L. D.; Xu, C. S. Role of Heat Shock Protein 27 Phosphorylation in Migration of Vascular Smooth Muscle Cells. *Mol. Cell. Biochem.* **2009**, *327*, 1–6.
25. Dreiza, C. M.; Brophy, C. M.; Komalavilas, P.; Furnish, E. J.; Joshi, L.; Pallero, M. A.; Murphy-Ullrich, J. E.; von Rechenberg, M.; Ho, Y. S.; Richardson, B.; et al. Transducible Heat Shock Protein 20 (HSP20) Phosphopeptide Alters Cytoskeletal Dynamics. *FASEB J.* **2005**, *19*, 261–263.
26. Hedges, J. C.; Dechert, M. A.; Yamboliev, I. A.; Martin, J. L.; Hickey, E.; Weber, L. A.; Gerthoffer, W. T. A Role for p38-(MAPK)/HSP27 Pathway in Smooth Muscle Cell Migration. *J. Biol. Chem.* **1999**, *274*, 24211–24219.
27. Guay, J.; Lambert, H.; Gingrasbreton, G.; Lavoie, J. N.; Huot, J.; Landry, J. Regulation of Actin Filament Dynamics by p38 MAP Kinase-Mediated Phosphorylation of Heat Shock Protein 27. *J. Cell Sci.* **1997**, *110*, 357–368.
28. Bakin, A. V.; Rinehart, C.; Tomlinson, A. K.; Arteaga, C. L. P38 Mitogen-Activated Protein Kinase Is Required for TGFβ-Mediated Fibroblastic Transdifferentiation and Cell Migration. *J. Cell Sci.* **2002**, *115*, 3193–3206.
29. Furnish, E. J.; Brophy, C. M.; Harris, V. A.; Macomson, S.; Winger, J.; Head, G. A.; Shaver, E. G. Treatment with Transducible Phosphopeptide Analogues of the Small Heat Shock-Related Protein, HSP20, after Experimental Subarachnoid Hemorrhage: Prevention and Reversal of Delayed Decreases in Cerebral Perfusion. *J. Neurosurg.* **2010**, *112*, 631–639.
30. Flynn, C. R.; Brophy, C. M.; Furnish, E. J.; Komalavilas, P.; Tessier, D.; Thresher, J.; Joshi, L. Transduction of Phosphorylated Heat Shock-Related Protein 20, HSP20, Prevents Vasospasm of Human Umbilical Artery Smooth Muscle. *J. Appl. Physiol.* **2005**, *98*, 1836–1845.
31. Hayess, K.; Benndorf, R. Effect of Protein Kinase Inhibitors on Activity of Mammalian Small Heat-Shock Protein (HSP25) Kinase. *Biochem. Pharmacol.* **1997**, *53*, 1239–1247.
32. Ward, B.; Seal, B. L.; Brophy, C. M.; Panitch, A. Design of a Bioactive Cell-Penetrating Peptide: When a Transduction Domain Does More Than Transduce. *J. Pept. Sci.* **2009**, *15*, 668–674.
33. Muto, A.; Panitch, A.; Kim, N.; Park, K.; Komalavilas, P.; Brophy, C. M.; Dardik, A. Inhibition of Mitogen Activated Protein Kinase Activated Protein Kinase II with MMI-0100 Reduces Intimal Hyperplasia *ex Vivo* and *in Vivo*. *Vasc. Pharmacol.* **2012**, *56*, 47–55.
34. Ruttekolk, I. R.; Witsenburg, J. J.; Glauner, H.; Bovee-Geurts, P. H. M.; Ferro, E. S.; Verdurmen, W. P. R.; Brock, R. The Intracellular Pharmacokinetics of Terminally Capped Peptides. *Mol. Pharmaceutics* **2012**, *9*, 1077–1086.
35. Lackey, C. A.; Press, O. W.; Hoffman, A. S.; Stayton, P. S. A Biomimetic pH-Responsive Polymer Directs Endosomal Release and Intracellular Delivery of an Endocytosed Antibody Complex. *Bioconjugate Chem.* **2002**, *13*, 996–1001.
36. Murthy, N.; Robichaud, J. R.; Tirrell, D. A.; Stayton, P. S.; Hoffman, A. S. The Design and Synthesis of Polymers for Eukaryotic Membrane Disruption. *J. Controlled Release* **1999**, *61*, 137–143.

37. Foster, S.; Duvall, C. L.; Crownover, E. F.; Hoffman, A. S.; Stayton, P. S. Intracellular Delivery of a Protein Antigen with an Endosomal-Releasing Polymer Enhances CD8 T-Cell Production and Prophylactic Vaccine Efficacy. *Bioconjugate Chem.* **2010**, *21*, 2205–2212.
38. Albarran, B.; Hoffman, A. S.; Stayton, P. S. Efficient Intracellular Delivery of a Pro-apoptotic Peptide with a pH-Responsive Carrier. *React. Funct. Polym.* **2011**, *71*, 261–265.
39. Liu, X. Y.; Fagotto, F. A Method To Separate Nuclear, Cytosolic, and Membrane-Associated Signaling Molecules in Cultured Cells. *Sci. Signaling* **2011**, *4*, pl2.
40. Yu, S. S.; Lau, C. M.; Barham, W. J.; Onishko, H. M.; Nelson, C. E.; Li, H.; Smith, C. A.; Yull, F. E.; Duvall, C. L.; Giorgio, T. D. Macrophage-Specific RNA Interference Targeting *via* "Click", Mannosylated Polymeric Micelles. *Mol. Pharmaceutics* **2013**, *10*, 975–987.
41. Accardo, A.; Aloj, L.; Aurilio, M.; Morelli, G.; Tesauro, D. Receptor Binding Peptides for Target-Selective Delivery of Nanoparticles Encapsulated Drugs. *Int. J. Nanomed.* **2014**, *9*, 1537–1557.
42. Li, H.; Miteva, M.; Kirkbride, K. C.; Cheng, M. J.; Nelson, C. E.; Simpson, E. M.; Gupta, M. K.; Duvall, C. L.; Giorgio, T. D. Dual MMP7-Proximity-Activated and Folate Receptor-Targeted Nanoparticles for siRNA Delivery. *Biomacromolecules* **2015**, *16*, 192–201.
43. Heitz, F.; Morris, M. C.; Divita, G. Twenty Years of Cell-Penetrating Peptides: From Molecular Mechanisms to Therapeutics. *Br. J. Pharmacol.* **2009**, *157*, 195–206.
44. Patel, L. N.; Zaro, J. L.; Shen, W. C. Cell Penetrating Peptides: Intracellular Pathways and Pharmaceutical Perspectives. *Pharm. Res.* **2007**, *24*, 1977–1992.
45. Li, H.; Nelson, C. E.; Evans, B. C.; Duvall, C. L. Delivery of Intracellular-Acting Biologics in Pro-apoptotic Therapies. *Curr. Pharm. Des.* **2011**, *17*, 293–319.
46. Cheng, Z. L.; Al Zaki, A.; Hui, J. Z.; Muzykantov, V. R.; Tsourkas, A. Multifunctional Nanoparticles: Cost *versus* Benefit of Adding Targeting and Imaging Capabilities. *Science* **2012**, *338*, 903–910.
47. Hevey, R.; Ling, C. C. Global Financial Challenge: Opportunities for Strengthening R&D Research in Targeted Drug Delivery. *Future Med. Chem.* **2012**, *4*, 1–5.
48. Ferrito, M. A.; Tirrell, D. A. Poly(2-ethylacrylic acid). *Macromolecular Syntheses*; Wiley: New York, 1992; Vol. 11, pp 59–62.
49. Convertine, A. J.; Benoit, D. S.; Duvall, C. L.; Hoffman, A. S.; Stayton, P. S. Development of a Novel Endosomolytic Diblock Copolymer for siRNA Delivery. *J. Controlled Release* **2009**, *133*, 221–229.
50. Elosegui-Artola, A.; Jorge-Penas, A.; Moreno-Arotzena, O.; Oregi, A.; Lasa, M.; Garcia-Aznar, J. M.; De Juan-Pardo, E. M.; Aldabe, R. Image Analysis for the Quantitative Comparison of Stress Fibers and Focal Adhesions. *PLoS One* **2014**, 10.1371/journal.pone.0107393.
51. Hocking, K. M.; Brophy, C.; Rizvi, S. Z.; Komalavilas, P.; Eagle, S.; Leacche, M.; Balaguer, J. M.; Cheung-Flynn, J. Detrimental Effects of Mechanical Stretch on Smooth Muscle Function in Saphenous Veins. *J. Vasc. Surg.* **2011**, *53*, 454–460.